Published in final edited form as:
Retina. 2009 October ; 29(9): 1356–1363. doi:10.1097/IAE.0b013e3181a5e657.

Ocular wavefront aberrations in patients with macular diseases

Kenichiro Bessho, MD[1,2], **Dirk-Uwe G. Bartsch, PhD**[1], **Laura Gomez, MD**[1,3], **Lingyun Cheng, MD**[1], **Hyoung Jun Koh, MD**[1], and **William R. Freeman, MD**[1]

[1]Department of Ophthalmology, University of California San Diego, Jacobs Retina Center/Shiley Eye Center, La Jolla, California

[2]Department of Visual Science, Osaka University Graduate School of Medicine, Suita, Osaka, Japan

[3]CODET ARIS Eye Institute, Tijuana, Mexico

Abstract

Background—There have been reports that by compensating for the ocular aberrations using adaptive optical systems it may be possible to improve the resolution of clinical retinal imaging systems beyond what is now possible. In order to develop such system to observe eyes with retinal disease, understanding of the ocular wavefront aberrations in individuals with retinal disease is required.

Methods—82 eyes of 66 patients with macular disease (epiretinal membrane, macular edema, macular hole etc.) and 85 eyes of 51 patients without retinal disease were studied. Using a ray-tracing wavefront device, each eye was scanned at both small and large pupil apertures and Zernike coefficients up to 6th order were acquired.

Results—In phakic eyes, 3rd order root mean square errors (RMS) in macular disease group were statistically greater than control, an average of 12% for 5mm and 31% for 3mm scan diameters ($p<0.021$). In pseudophakic eyes, there also was an elevation of 3rd order RMS, on average 57% for 5mm and 51% for 3mm scan diameters ($p<0.031$).

Conclusion—Higher order wavefront aberrations in eyes with macular disease were greater than in control eyes without disease. Our study suggests that such aberrations may result from irregular or multiple reflecting retinal surfaces. Modifications in wavefront sensor technology will be needed to accurately determine wavefront aberration and allow correction using adaptive optics in eyes with macular irregularities.

Keywords

Macular disease; Ray tracing; Retinal imaging; Wavefront aberration

Introduction

Retinal imaging is an important objective method to assess retinal structure and integrity, study retinal disease, visualize the ocular circulation and monitor the effect of treatment on

Reprint Request: Dirk-Uwe G. Bartsch PhD dbartsch@ucsd.edu Shiley Eye Center, 9415 Campus Point Drive, La Jolla, CA 92093-0946 Phone: 858-534-3513 FAX: 858-534-7985.

No author has any proprietary interest.

Brief Summary The ocular wavefront contains more aberrations in eyes with macular disease. Such wavefront aberrations will limit the use of adaptive optical compensation unless they can be corrected for in imaging systems designed to use adaptive optics to improve the imaging of the macula.

retinal disease. The resolution of retinal photographic equipment is limited by the optical power of the last imaging lens - the human eye. The many imperfections in the human eye include chromatic aberrations, coma, spherical aberrations, astigmatism, and higher order aberrations. Thus, the transverse resolution in retinal photography is in the order of 15 to 20 microns while the axial or longitudinal resolution in confocal SLO of the eye is in the order of 300 to 450 microns.1

There are several areas of ophthalmology where high-resolution imaging will offer significant benefits. These areas include ocular melanoma, tumor vessel characterization,2 age-related macular degeneration, choroidal neovascularization, diabetic retinopathy, AIDS, glaucoma, study of macular vitreoretinal interface disorders and retinal thickness measurement. Development of high-resolution fundus imaging will improve our understanding and possibly treatment of many retinal disorders.

Several groups have suggested that by compensating for ocular aberrations using adaptive optical systems3–8 it may be possible to improve the resolution of clinical retinal imaging systems. One potential advantage of compensating for ocular aberrations is the ability to directly observe the photoreceptors and microscopic pathologic structures. In healthy human eyes, there have been reports that this may be possible in optimal conditions.3,5–7 The ability to image the photoreceptors, RPE cells and other structures would have important research and clinical implications relating to disease detection and treatment and understanding pathophysiology. For these reasons, it is important to understand the ocular aberrations present in human eyes with retinal disease. One group of diseases for which improved imaging might be very important is macular diseases. We therefore undertook a study of patients with a variety of macular pathologies. Understanding the range of and types of wavefront aberrations present is an important step in developing devices to compensate for these aberrations and allow improved imaging of normal and pathological eyes.

Subjects and Methods

Patient Characteristics

The study population consisted of 80 eyes of 66 patients with retinal disease (36 male, 30 female), of these 37 eyes were phakic and 43 were pseudophakic. For controls, 78 eyes of 49 patients without retinal disease (18 male, 31 female) were imaged, of these 44 eyes were phakic and 34 were pseudophakic. There was no statistical difference between disease and control group in age and conventional refraction except for cylinder in pseudophakic study [Table 1].

Table 2 lists the retinal diseases that were present. In all cases, patients had clinically diagnosed macular disease that caused irregularity of the retinal surface. Choroidal neovascularization (CNV) included subretinal hemorrhage and pigment epithelium detachment, with or without exudative retinal detachment, and macular edema (ME) induced by pseudophakia, retinal vein occlusion, diabetic retinopathy or uveitis. Diseases with associated vitreous opacity were excluded, as well as optically significant cataract, apparent dislocation of the intraocular lens or any eye surgery within six months prior to measurement.

Methods

In all cases, ocular wavefront aberrations were measured using the Tracey Visual Function Analyzer (VFA software version 1.0, Tracey Technologies, Houston, TX), which is based on ray-tracing principle.9–14

The device projects 64 light rays located in 4 concentric circles across the pupil in succession and detects the retinal location of reflection within 0.06 seconds with the help of two linear charged coupled device (CCD) arrays. Based on these measurements the device calculates the retinal point spread function (PSF) and subsequently the wavefront aberrations. Conventional refractive indexes are also generated by reverse calculation of Zernike coefficients and therefore depend on the analysis area size. A single measurement constitutes a complete examination for each eye. In a recent unpublished study we measured the reproducibility of the VFA and found that the Root Mean Square (RMS) of Zernike terms had a ratio of standard deviation to mean measurement value of 57%. The results were similar to the findings by other researchers when comparing the reading of conventional refraction.9,13–15

The VFA has an automatic acquisition mode that measures wavefront at maximum available pupil size as a default setting, as well as a manual mode in which area size is adjustable. Each eye was scanned at maximum pupil size in early part of the study, and subsequently pupil size was fixed to 3mm and 6mm diameters for phakic and 5mm diameters for pseudophakic eyes. Each patient eye was dilated using 2–3 sets of 1% tropicamide and 2.5% phenylephrine eye drops before measurement, and for both scan sizes wavefront was measured two to four times by one examiner [KB]. From the data one best scan was selected for each scan size respectively by one reviewer [KB]. In cases where the clear optical zone of the intraocular lens implant was small, or the pupil was small, the scanning area was restricted and therefore less number of the eye was available for the large scan area study.

Data of 25 Zernike coefficients (2nd to 6th order) were downloaded onto computer software (Microsoft Excel v.X, Microsoft, Redmond, WA) for both small and large scans. From 3mm scan data conventional refraction data (Sph, Cyl, Ax) were also downloaded.

Several reports have described that wavefront values depend on the size of analysis area.16–19 To compare the data scanned at different pupil size, it has been suggested to mathematically transforming the data into a unified pupil size.16,17 The equation described by Schwiegerling17 is as follows (modified by author [KB] for use of coefficients up to 6th order);

$$b_{2m}=\frac{r_2^2}{r_1^2}\left[a_{2m}-a_{4m}\sqrt{15}\left(1-\frac{r_2^2}{r_1^2}\right)+a_{6m}\sqrt{21}\left(2-5\frac{r_2^2}{r_1^2}+3\frac{r_2^4}{r_1^4}\right)\right]$$

$$b_{3m}=\frac{r_2^3}{r_1^3}\left[a_{3m}-a_{5m}2\sqrt{6}\left(1-\frac{r_2^2}{r_1^2}\right)+a_{7m}\sqrt{8}\left(5-12\frac{r_2^2}{r_1^2}+7\frac{r_2^4}{r_1^4}\right)\right]$$

$$b_{4m}=\frac{r_2^4}{r_1^4}\left[a_{4m}-a_{6m}\sqrt{35}\left(1-\frac{r_2^2}{r_1^2}\right)\right]$$

$$b_{5m}=\frac{r_2^5}{r_1^5}a_{5m}$$

$$b_{6m}=\frac{r_2^6}{r_1^6}a_{6m}$$

where a_{nm} is an original Zernike coefficient, b_{nm} is a new coefficient, r_1 is an original radius of analysis area, r_2 is a new radius to be transformed. Coefficients are described in double index scheme; n and m indicate radial order and spatial frequency, respectively. This equation cannot predict the wavefront of larger analysis area, thus the new, unified analysis area is limited to be smaller than the original area.

Using this equation all large scan size measurement data were transformed to that of 5mm diameter. For small scan size measurement, since it was designed to perform at constant 3mm scan size, non-transformed data were used.

The root mean square (RMS) errors for each Zernike term were calculated, as well as several combined indexes shown in Tables 3 and 4.

S2 to S6 indicate the root mean square value (RMS) of the 2nd (C3 to C5), through 6th (C21 to C27) order Zernike coefficients individually. The total HO is the RMS of higher order terms (C6 to C27); the total RMS is the RMS of all 25 Zernike terms.

Statistical analysis was performed using another computer software (JMP IN ver. 4.0.2, SAS institute inc. Cary, NC).

Effect of eccentric fixation on wavefront error

In order to test the hypothesis that eccentric fixation at the juxtamacular area that might occur in patients with macular disease would cause an increase in wavefront abnormalities, we tested four normal healthy individuals without macular pathology. In each case, the subject was asked to fixate on the internal fixation target of the instrument, simultaneously co-locating another target (A) at a 1m distance using the fellow eye. The distant target (A) was placed so that subjectively it was overlapped on the internal target image. Wavefront measurements were done using fellow eye fixation. Eccentric fixation testing was done using fellow eye fixation and a target (B), 8.7cm apart from the initial target (A) for 5-degrees of eccentricity, another target (C) that was 17.6cm apart was used for 10-degrees of eccentricity. Data was acquired using the same protocol as above. A comparison of the Zernike polynomials was made in the three positions.

Results

Phakic Eye Study

In eyes with macular disease, total RMS (RMS of 25 Zernike coefficients) ranged from 0.144 to 7.377μm (2.545±1.625 (5mm scan), 1.044±0.729 (3mm scan), Mean±SD), total higher order RMS (Total HO: RMS of C6 to C27) ranged from 0.054 to 1.858μm (0.422±0.281 (5mm scan), 0.140±0.081 (3mm scan)). Table 3 shows the difference of RMS error between phakic patients with normal maculae and those with macular disease. Eyes with macular disease had greater wavefront aberrations than normal in most wavefront indexes. The wavefront differences ranged from −0.4% to 62% of the values in the normals, and differences were statistically significant for 3rd order and total higher order RMS for both scan sizes. For the other RMS values the trend almost consistently indicated that macular irregularities were associated with higher wavefront abnormalities.

Pseudophakic eye study

Table 4 shows the difference in RMS error between patients who had an IOL implant with a normal macula and those with macular disease. Total RMS ranged from 0.167 to 3.910μm (2.158±0.785 (5mm scan), 0.745±0.401 (3mm scan), Mean±SD), and total higher order RMS (Total HO) ranged from 0.037 to 1.942μm (0.656±0.368 (5mm scan), 0.223±0.182 (3mm scan)). Eyes with macular disease had greater wavefront aberrations than eyes with normal maculae in most wavefront indexes. The wavefront differences ranged from 12% to 93% of the values in the normals, and these differences were statistically significant for 2nd and 3rd, total higher order RMS and total RMS for both scan diameters. For the other RMS values the trend consistently indicated that macular irregularities were associated with higher wavefront abnormalities.

For both phakic and pseudophakic studies with both scan sizes the 3rd order RMS value was always statistically higher in the eyes with macular disease (S3, P<0.021). Table 5 shows the detailed profile of the 3rd order indexes that comprise S3. All indexes were greater in the macular disease group than controls, however, difference was not significant.

Effect of eccentric fixation on wavefront error

The total RMS value of the centric, 5- and 10-degree eccentric fixation control subjects was 0.492±0.315, 0.516±0.248 and 0.604±0.247 (p=0.625 for 0 deg vs. 5deg, 0.375 for 0 deg vs. 10 deg. Paired Wilcoxon rank-sum test). Similarly there was no difference between the groups in individual RMS Zernike terms (Table 6).

In addition, in analyzing the main study data, we reviewed the stored photographs of the pupil and the corneal reflex of four reference markers to determine whether patients with and without macular disease did fixate centrally at the moment of data acquisition. In all cases, we were not able to document fixation failure.

Discussion

In order to use adaptive optics to improve the ability to image the retina, it is necessary to obtain data on the wavefront aberrations of each subject's eye and to compensate for these aberrations.3,4,6–8 All currently available wavefront sensing systems are double-pass systems that assume an essentially flat, regular posterior pole of the eye. In order to determine the wavefront of an individual eye, these systems rely on one of several techniques to measure the wavefront.

The Tscherning aberroscope projects a grid of points onto the retina, the distortion of the grid of points is photographed and from this, wavefront aberrations are calculated.20 The Hartmann-Shack wavefront sensor technique relies on the projection of a point source light on the retina. The light reflected from this point on the retina is imaged onto a lenslet array and sampled with a CCD chip. Wavefront aberrations are calculated assuming that a point of light on the retina was the origin of the image.11 The Skiaskopy technique effectively performs retinoscopy at multiple points over the pupil and from these data, multiple refractive errors the wavefront over the entire exit pupil is calculated.12 The laser ray-tracing technique, which we employed in this study uses projection of a thin infrared laser beam onto the retina and detects the location of reflection one by one in succession. This is sequentially completed over 64 sampling points within 0.06 seconds so that the eye movement does not effect the measurement. The merit of this technique is that it can detect larger magnitude errors of reflection than Hartmann-Shack methods, and that it is more rapid and sensitive than the Tscherning methods that essentially require averaging of data from each sampling point.

We studied pseudophakic and phakic patients separately because pseudophakic eyes have different internal optics and there have been reports suggesting that pseudophakic eyes have different wavefront values.21–23 Indeed there was a difference in wavefront results between pseudophakic and phakic patients for both small and large pupil diameters. In general, pseudophakic eyes had higher wavefront errors (S3–S6) with the exception of astigmatism (Z3+Z5 or S2-defocus) and defocus (Z4) that are probably minimized in pseudophakic eyes by cataract surgery and the associated intraocular lens implant (Table 7). This was consistent with clinical studies suggesting more higher-order aberrations in pseudophakic eyes, although it should be considered that the pseudophakic group in our study was made up of a significantly older population than the phakic group (See Table 1).

In our study we noted that for both small and large pupils, in both pseudophakic and phakic eyes, the wavefront error in eyes with macular disease was larger for all parameters than that in eyes without macular disease. In approximately one third of the studied values this was statistically significant, and in the remainder there was a trend in this direction. One possible explanation might be that eyes with macular disease fixated eccentrically.24 We ruled this out by studying eccentric fixation in a group of normal subjects and found that paramacular fixation did not affect the wavefront values. In addition, all measurements were performed by one examiner checking patient's fixation, and moreover, in review of the pupil images taken at the time of measurements, we found no obvious eccentric fixation in our cohort.

Another explanation is that the micro-displacement of the intraocular optics especially in pseudophakic eyes. It may be possible that focal intraocular proliferation in eyes with retinal disease results in tilt or decentration of the lens implant. However, the elevation of the 3rd order RMS was observed throughout pseudophakic and phakic study.

We conclude that irregular focal elevation or depression of the retina in or near the posterior pole of the eye will cause wavefront abnormalities because many wavefront sensing devices designed for use in the human eye assume a smooth reflecting surface that is not present in eyes with macular disease and retinal surface irregularities. Histopathology of eyes with CNV for example shows the irregularities of the retinal surface yielding peak elevations spaced at intervals between 30 and 360 microns.25,26 Figure 1 shows how an irregular retinal surface would adversely effect on wavefront aberrations in either device with a small retinal sampling area (around 100 microns diameter in devices such as a Hartmann-Shack wavefront sensor) or wavefront sensors that require a large retinal sampling area (Tscherning aberroscopy, laser ray tracing or skiascopy). In both cases eyes with irregular retinal surface profiles with or without multiple retinal and subretinal optical interfaces blur the wavefront image and have a degrading effect on light reflection for all wavefront sensors. In this study we only evaluated one of the four types of wavefront sensors currently available. Future studies in patients with macular diseases will allow us to determine which technique is less affected by macular irregularities.

For these reasons, new techniques will have to be developed to allow accurate wavefront measurements without this assumption. This is important because the ability to apply adaptive optics to retinal imaging will be particularly important in eyes with macular disease. It is possible that certain existing techniques will be less effected by macular irregularities. Of the four techniques in clinical use, Tscherning aberroscopy, skiascopy and ray tracing devices utilize a larger retinal image area to generate wavefront measurements. In contrast, the Hartmann-Shack techniques may use a smaller area on the order of 50–100 microns that may be particularly susceptible to distortions of macular topography at a given measurement. However, our study only analyzed the effect of macular irregularities on one of these instruments. The effect of macular irregularities on the three other instruments (skiascopy, Tscherning aberroscopy and Hartmann-Shack wavefront sensing) needs to be investigated. At the current time, retinal cameras are not incorporated into these instruments but such a camera could aid the operator to find a flat imaging area.

Acknowledgments

This study was supported in part by a grant from the Osaka Medical Research Foundation for Incurable Diseases, Osaka Japan, (Bessho K), National Eye Institute NIH-NEI grant #EY13304 (Bartsch DU) and NIH grant #EY07366 (Freeman WR).

References

1. Bartsch DU, Freeman WR. Axial Distribution Analysis of the Human Retina with a Confocal Scanning Laser Tomograph. Exp Eye Research. 1994; 58:161–173.
2. Mueller AJ, Bartsch DU, Folberg R, Mehaffey MG, Boldt HC, Meyer M, Gardner LM, Goldbaum MH, Pe'er J, Freeman WR. Imaging the microvasculature of choroidal melanomas with confocal indocyanine green scanning laser ophthalmoscopy. Arch Ophthalmology. 1998; 116(1):31–9.
3. Roorda A. Adaptive Optics Ophthalmoscopy. J Refract Surgery. Sep-Oct;2000 16:S602–7.
4. Bartsch DU, Zhu L, Sun PC, Fainman S, Freeman WR. Retinal imaging with a low-cost micromachined membrane deformable mirror. J Biomed Opt. Jul; 2002 7(3):451–6. [PubMed: 12175296]
5. Cheng L, Singer B, Guirao A, Porter J, Williams DR. Image metrics for predicting subjective image quality. Optom Vis Sci. May; 2005 82(5):358–69. [PubMed: 15894912]
6. Roorda A, Metha AB, Lennie P, Williams DR. Packing arrangement of the three cone classes in primate retina. Vision Research. 2001; 41(10–11):1291–306. [PubMed: 11322974]
7. Roorda A, Romero-Borja F, Donnelly WJ III, Hebert TJ, Campbell MCW. Adaptive optics scanning laser ophthalmoscopy. Optic Express. 2002; 10(9):405–412.
8. Liang J, Williams DR, Miller DT. Supernormal vision and high-resolution retinal imaging through adaptive optics. J Opt Soc Am A. Nov; 1997 14(11):2884–92.
9. Wang L, Misra M, Pallikaris IG, Koch DD. Comparison of a ray-tracing refractometer, autorefractor, and computerized videokeratography in measuring pseudophakic eyes. J Cataract Refract Surgery. Feb; 2002 28(2):276–82.
10. Moreno-Barriuso E, Marcos S, Navarro R, Burns SA. Comparing laser ray tracing the spatually resolved refractometer, and the Hartmann-Shack sensor to measure the ocular wave aberration. Optom Vis Sci. Mar; 2001 78(3):152–156. [PubMed: 11327676]
11. Moreno-Barriuso E, Navarro R. Laser Ray Tracing versus Hartmann-Shack sensor for measuring optical aberrations in the human eye. J Opt Soc Am A. 2000; 17(6):974–985.
12. Buscemi P. Clinical applications of the OPD-Scan wavefront aberrometer/corneal topographer. J Refract Surgery. May-Jun;2002 18(3suppl):S385–8.
13. Pallikaris IG, Panagopoulou SI, Molebny VV. Clinical experience with the Tracey technology wavefront device. J Refract Surgery. Sep-Oct;2000 16(5):S588–91.
14. Wang L, Wang N, Koch DD. Evaluation of refractive error measurements of the Wavescan Wavefront system and the Tracey Wavefront aberrometer. J Cataract Refract Surgery. May; 2003 29(5):970–9.
15. Salmon TO, West RW, Gasser W, Kenmore T. Measurement of refractive errors in young myopes using the COAS Shack-Hartmann aberrometer. Optom Vis Sci. Jan; 2003 80(1):6–14. [PubMed: 12553539]
16. Campbell CE. Matrix method to find a new set of Zernike coefficients from an original set when the aperture radius is changed. J Opt Soc Am A Opt Image Sci Vis. Feb; 2003 20(2):209–217. [PubMed: 12570287]
17. Schwiegerling J. Scaling Zernike expansion coefficients to different pupil sizes. J Opt Soc Am A. 2002; 19(10):1937–1945.
18. Goldberg KA, Geary K. Wave-front measurement errors from restricted concentric subdomains. J Opt Soc Am A Opt Image Sci Vis. Sep; 2001 18(9):2146–2152. [PubMed: 11551047]
19. Wang Y, Zhao K, Jin Y, Niu Y, Zuo T. Changes of higher order aberration with various pupil sizes in the myopic eye. J Refract Surgery. Mar-Apr;2003 19(2 Suppl):S270–274.
20. Kaemmerer M, Mrochen M, Mierdel P, Krinke HE, Seiler T. Clinical experience with the Tscherning aberrometer. J Refract Surgery. Sep-Oct;2000 16:S584–587.
21. Guirao A, Redondo M, Geraghty E, Piers P, Norrby S, Artal P. Corneal optical aberrations and retinal image quality in patients in whom monofocal intraocular lenses were implanted. Arch Ophthalmology. Sep; 2002 120(9):1143–51.
22. Miller JM, Anwaruddin R, Straub J, Schwiegerling J. Higher order aberrations in normal, dilated, intraocular lens, and laser in situ keratomileusis corneas. J Refract Surgery. Sep-Oct;2002 18(5):S579–83.

23. Mierdel P, Kaemmerer M, Krinke HE, Seiler T. Effects of photorefractive keratectomy and cataract surgery on ocular optical errors of higher order. Graefes Arch Clin Exp Ophthalmology. 1999; 237(9):725–9.

24. Rynders MC, Navarro R, Losada MA. Objective measurement of the off-axis longitudinal chromatic aberration in the human eye. Vision Research. Feb; 1998 38(4):513–22. [PubMed: 9536375]

25. Green WR, Enger C. Age-related macular degeneration histopathologic studies. The 1992 Lorenz E. Zimmerman Lecture. Ophthalmology. 1993; 100(10):1519–35. [PubMed: 7692366]

26. Grossniklaus HE, Gass JD. Clinicopathologic correlations of surgically excised type 1 and type 2 submacular choroidal neovascular membranes. Am J Ophthalmology. Jul; 1998 126(1):59–69.

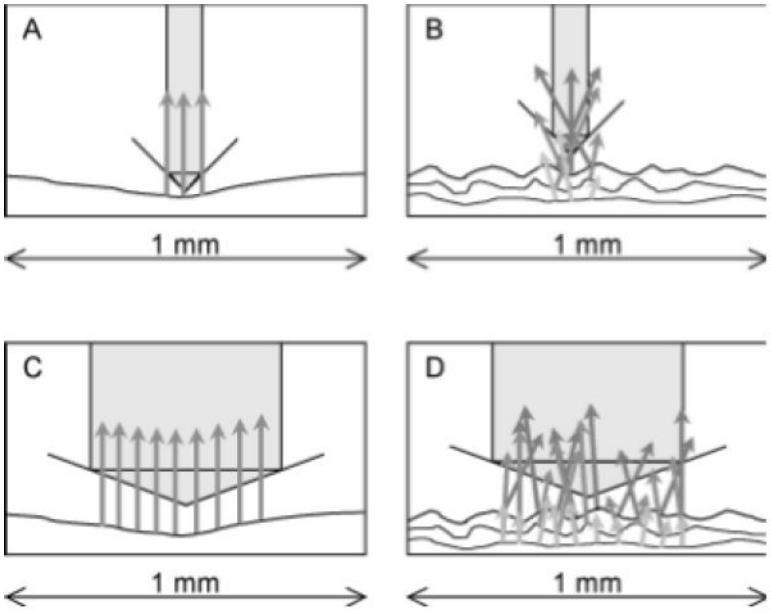

Figure 1.

Diagram of the light reflection at normal and irregular retinal surfaces for small and large retinal measurement area. Figure 1A shows the possible light reflection in a normal eye with a wavefront sensor that uses a small retinal area for light reflection. Figure 1B shows the possible explanation of light reflection in a diseased eye with the same type of wavefront sensors. Figure 1C shows the possible light reflection in a normal eye with a wavefront sensor that uses a large retinal area for light reflection, while Figure 1D shows the possible explanation of light reflection in a diseased eye.

Table 1

Number, age and conventional refraction of eyes studied

Phakic	Macular Disease	Control	P*
Eyes/Patients	36/32	44/28	
Age	65.7±11.1yo	63.8±14.0yo	0.493
Sph	0.2±3.0D	0.1±2.7D	0.801
Cyl	−1.4±0.8D	−1.3±0.8D	0.559
Spherical Equivalent	−0.4±3.2D	−0.6±2.7D	0.877

Pseudophakic	Macular Disease	Control	P*
Eyes/Patients	44/34	33/21	
Age	74.5±12.3yo	75.7±8.3yo	0.644
Sph	0.2±1.8D	0.6±0.8D	0.233
Cyl	−1.8±1.1D	−1.0±0.7D	**0.001**
Spherical Equivalent	−0.7±1.8D	0.1±0.9D	**0.019**

Mean±SD

*ANOVA

Table 2

Number and type of macular lesions studied (3mm)

Disease	Lens Status	N
Macular Edema	Phakic	13
	Pseudophakic	11
Choroidal Neovascularization	Phakic	4
	Pseudophakic	8
Epiretinal Membrane	Phakic	10
	Pseudophakic	6
Geographic Atrophy	Phakic	1
	Pseudophakic	8
Macular Hole	Phakic	2
	Pseudophakic	5
Macular Scar	Phakic	6
	Pseudophakic	6
Total		80

Table 3

Comparison of wavefront in phakic eyes

Scan: 5mm	Disease Total	Control 1	%Difference*	P†
S2	2.466±1.668	2.476±2.109	−0.4%	0.492
S2 -defocus	0.823±0.572	0.770±0.484	6.8%	0.882
S3	0.175±0.074	0.156±0.097	12.3%	**0.021**
S4	0.059±0.067	0.037±0.029	61.9%	0.071
S5	0.034±0.049	0.026±0.024	29.1%	**0.015**
S6	0.373±0.280	0.279±0.161	33.9%	0.607
Total HO	0.422±0.281	0.328±0.176	28.8%	**0.019**
Total RMS	2.545±1.625	2.506±2.106	1.6%	0.350

Scan: 3mm	Disease Total	Control 1	%Difference*	P†
S2	1.03±0.73	0.854±0.503	20.7%	0.332
S2 -defocus	0.337±0.17	0.291±0.172	15.9%	0.201
S3	0.123±0.073	0.094±0.053	31.1%	**0.009**
S4	0.052±0.042	0.047±0.033	11.0%	0.364
S5	0.019±0.017	0.016±0.012	19.9%	0.616
S6	0.013±0.012	0.013±0.012	6.0%	0.654
Total HO	0.14±0.081	0.11±0.059	27.0%	**0.017**
Total RMS	1.044±0.729	0.863±0.502	20.9%	0.289

Mean±SD

S2: RMS of C3 to C5 (2^{nd} order indexes), S2-Defocus: RMS of C3 and C5, S3: RMS of C6 to C9 (3^{rd} order indexes), S4: RMS of C10 to C14 (4^{th} order indexes), S5: RMS of C15 to C20 (5^{th} order indexes), S6: RMS of C21 to C27 (6^{th} order indexes), Total HO: RMS of S3 to S6, Total RMS: RMS of S2 to S6

*%(Disease-Control1)/control1

†ANOVA on logarithm of each value

Table 4

Comparison of wavefront in pseudophakic eyes

Scan: 5mm	Disease Total	Control 2	%Difference*	P†
S2	2.021±0.792	1.046±0.355	93.2%	**0.001**
S2 -defocus	1.216±0.685	0.749±0.312	62.3%	**0.016**
S3	0.517±0.321	0.329±0.155	57.4%	**0.009**
S4	0.289±0.193	0.257±0.073	12.4%	0.923
S5	0.162±0.180	0.105±0.091	53.9%	0.210
S6	0.096±0.097	0.070±0.048	36.1%	0.477
Total HO	0.656±0.368	0.460±0.132	42.8%	**0.024**
Total RMS	2.158±0.785	1.156±0.335	86.7%	**0.001**

Scan: 3mm	Disease Total	Control 2	%Difference*	P†
S2	0.677±0.419	0.368±0.185	84.1%	**0.001**
S2 -defocus	0.423±0.282	0.244±0.172	73.8%	**0.006**
S3	0.176±0.155	0.117±0.067	51.0%	**0.031**
S4	0.108±0.102	0.068±0.047	58.7%	0.051
S5	0.042±0.042	0.025±0.016	66.5%	0.213
S6	0.032±0.033	0.02±0.013	60.0%	0.564
Total HO	0.223±0.182	0.144±0.075	54.5%	**0.026**
Total RMS	0.745±0.401	0.401±0.186	85.7%	**0.000**

*%(Disease-Control2)/control2

†ANOVA on logarithm of each value

Table 5

Profiles of 3rd order RMS

Phakic	Scan: 3mm			Scan: 5mm		
	Disease	Control	P*	Disease	Control	P*
Z6	0.057±0.040	0.04±0.036	0.054	0.263±0.372	0.135±0.138	0.082
Z7	0.055±0.046	0.053±0.043	0.919	0.288±0.430	0.224±0.251	0.243
Z8	0.043±0.048	0.03±0.025	0.295	0.195±0.197	0.133±0.125	0.322
Z9	0.055±0.063	0.041±0.03	0.460	0.181±0.176	0.136±0.143	0.344

Pseudo-phakic	Scan: 3mm			Scan: 5mm		
	Disease	Control	P*	Disease	Control	P*
Z6	0.066±0.074	0.051±0.039	0.804	0.246±0.319	0.160±0.127	0.629
Z7	0.080±0.120	0.066±0.053	0.718	0.301±0.248	0.194±0.173	0.338
Z8	0.081±0.101	0.045±0.045	**0.028**	0.236±0.210	0.112±0.075	0.257
Z9	0.066±0.057	0.040±0.037	0.067	0.147±0.107	0.097±0.074	0.487

*ANOVA on logarithm of each value

Retina. Author manuscript; available in PMC 2013 July 15.

Table 6

The effect of eccentric fixation on wavefront measurement

	Centered	5 deg	10 deg	P* vs. 5deg	P* vs. 10deg
S2	0.457±0.337	0.486±0.266	0.582±0.254	0.625	0.375
S2-Defocus	0.337±0.351	0.295±0.324	0.313±0.307	0.125	0.875
S3	0.116±0.060	0.125±0.043	0.132±0.027	0.875	0.625
S4	0.066±0.021	0.055±0.026	0.057±0.027	0.125	0.125
S5	0.022±0.008	0.022±0.004	0.026±0.003	0.875	0.625
S6	0.014±0.003	0.016±0.006	0.014±0.006	0.375	0.625
Total HO	0.139±0.058	0.141±0.049	0.148±0.037	0.875	0.625
Total RMS	0.492±0.315	0.516±0.248	0.604±0.247	0.625	0.375
Sph	−0.9±0.6D	−1.0±0.5D	−1.2±0.5D	0.625	0.250
cyl	0.8±0.8D	0.7±0.8D	0.8±0.7D	0.125	0.875
SphEq	−0.5±0.2D	−0.6±0.2D	−0.8±0.2D	0.250	0.125

No significant difference in all indexes

*Paired Wilcoxon Signed-Rank test on logarithm of each value

Table 7

Comparison of two controls of phakic (Control 1) and pseudophakic (Control 2) at 3mm scan

	Phakic	Pseudophakic	%Difference of mean*	P†
Sph	0.1±2.7	0.6±0.8	−83.6%	0.350
Cyl	−1.3±0.8	−1±0.7	30.9%	0.149
Spherical Equivalent	−0.6±2.7	0.1±0.9	−896.3%	0.229
S2	0.854±0.503	0.384±0.204	122.5%	**<0.001**
S2-Defocus	0.291±0.172	0.251±0.175	15.9%	0.205
S3	0.094±0.053	0.118±0.066	−20.1%	0.068
S4	0.047±0.033	0.071±0.050	−33.9%	**0.023**
S5	0.016±0.012	0.026±0.016	−38.8%	**0.003**
S6	0.013±0.012	0.020±0.013	−38.0%	**0.001**

*%(Phakic-Pseudophakic)/Pseudophakic

†ANOVA